Eur. Phys. J. D **1**, 149-163 (1998)

THE EUROPEAN PHYSICAL JOURNAL D

Multiconfiguration Dirac-Fock calculation of $2s_{1/2}-2p_{3/2}$ transition energies in highly ionized bismuth, thorium, and uranium

J.P. Santos[1], J.P. Marques[2], F. Parente[2], E. Lindroth[3], S. Boucard[4], and P. Indelicato[4,a]

[1] Departamento de Física da Universidade Nova de Lisboa, Centro de Física Atómica da Universidade de Lisboa, Av. Prof. Gama Pinto 2, 1699 Lisboa Codex, Portugal
[2] Departamento de Física da Universidade de Lisboa, Centro de Física Atómica da Universidade de Lisboa, Av. Prof. Gama Pinto 2, 1699 Lisboa Codex, Portugal
[3] Department of Atomic Physics, Stockholm University, 104 05 Stockholm, Sweden
[4] Laboratoire Kastler-Brossel Ecole Normale Supérieure et Université Pierre et Marie Curie[b], Boîte 74, 4 place Jussieu, 75252 Paris Cedex 05, France

Received: 5 November 1997 / Accepted: 8 December 1997

Abstract. Structure and QED effects for $2s_{1/2}$ and $2p_{3/2}$ levels are calculated for lithiumlike U^{89+} trough neonlike U^{82+}, lithiumlike Th^{87+} trough neonlike Th^{80+} and lithiumlike Bi^{80+} trough neonlike Bi^{73+}. The results of the first two sets are compared with recent measurements of the $2s_{1/2} - 2p_{3/2}$ transition energy in 3 to 10-electron ions. Good agreement with experiment is found for most of the observed lines. Forty-one possible transitions are calculated for each ion in the eight ionization states, in the experimental energy range. Twenty-eight of these transitions have not been observed, nor calculated previously. We also calculate transition rates, branching ratios, excitation and ionization cross sections and confirm that the thirteen experimental observed transitions correspond to the ones with highest relative intensities. However, we find nineteen more transitions that could be measured in a more sensitive experiment.

PACS. 32.70.Cs Oscillator strengths, lifetime, transition moments – 32.70.Fw Absolute and relative intensities – 31.25.-v Electron correlation calculations for atoms and molecules

1 Introduction

Recently, high-precision measurements of the $2s_{1/2}-2p_{3/2}$ transition energies in lithiumlike U^{89+} trough neonlike U^{82+} and lithiumlike Th^{87+} trough neonlike Th^{80+} were made at an Electron-Beam Ion Trap (Super-EBIT) at Lawrence Livermore Laboratory [1,2]. Since then, the uranium measurements, with the exception of the neonlike charge state, have been compared with the results from a calculation using the Relativistic Configuration-Interaction (RCI) method with B-splines basis functions [3] and revealed a discrepancy less than 1 eV. For the cases of lithiumlike, berylliumlike, carbonlike, fluorinelike, and neonlike uranium the energies have also been calculated by the Relativistic Many-Body Perturbation Theory (RMBPT) [4]. The energy values obtained using this method are quite close to the experimental ones, with the exception of berylliumlike and neonlike uranium. Yet RMBPT cannot easily tackle the problem of nitrogen-like and oxygen-like ions and RCI may not deal with more than 9 electrons because of the computer resources needed.

Reliable theoretical predictions of atomic levels require methods that account for electron correlation, relativistic, and quantum-electrodynamic (QED) corrections. The MCDF method [5–9] is one of the most flexible computational schemes to produce Self-Consistent-Field (SCF) wave functions that incorporate relativistic corrections and the major part of the electron correlation for atoms with simple and complex valence-shell configurations.

The purpose of this paper is to calculate all possible $2s_{1/2} - 2p_{3/2}$ transition energies in lithiumlike Th^{87+} trough neonlike Th^{80+} and lithiumlike U^{89+} trough neonlike U^{82+} and extend them to lithiumlike Bi^{80+} trough neonlike Bi^{73+}, using the MCDF method as implemented by Desclaux, Indelicato and collaborators [7–12] and make a critical assessment of the precision of the MCDF method, in a well defined case. This will enable to have a precise knowledge of the accuracy of MCDF calculations for more complicated ions (more than 10 electrons) for which both RCI and RMBPT are likely to fail (RMBPT will however always allow to do cases with closed shells with one extra electron or one hole).

The MCDF program we used has very advanced features that allow to treat residual terms, including Breit

[a] e-mail: paul@spectro.jussieu.fr
[b] Unité Associée au CNRS No. 18

interaction, all-order retardation, magnetic correlation, one-particle self-energy and vacuum polarization, and two-electron radiative corrections. This program also include full support for non-orthogonal orbitals between initial and final state for non-diagonal one-electron operators (transition probability...) using an approach different from the one used by Froese Fisher and collaborators (biorthogonal transformations [13], which works only on restricted classes of configurations subspace) and partial support for non-orthogonal orbitals inside a given state. For example we can include series of configurations like $1s2p + 2p'3d + 3d'4f \cdots$ for up to 4 electrons. Finally it is the only MCDF code to implement projection operators, and thus enables to do a correct treatment of negative energy continuum and correlation in strong field [12]. The price to pay is that calculations are very demanding in computer time and central memory, making it almost impossible to go over a few hundred jj configurations in any given calculation. Other MCDF codes [14,5] are able to achieve calculations with several thousands of configurations, but they do not implement projection operators, nor do they allow complete inclusion of the Gaunt (Magnetic Interaction) in the Self-Consistent Field process (it is included only in the Hamiltonian matrix but not in the wave function differential equation), thus limiting severely their usefulness at very high Z. An other limitation of the present code is that even though it allows the freedom of having non-orthogonal orbitals between correlation configurations, it does not implement an energy expression valid in the most general case. A full support of non orthogonal orbital has been implemented only for one-electron operators (transition probability, hyperfine structure...). To achieve a sizeable amount of correlation with limited configuration space we use the Optimized Level (OL) scheme, and achieve self-consistence for all occupied and correlation orbitals. It thus becomes often very hard or impossible to achieve convergence for very large number of configurations, even with powerful numerical methods to solve for individual orbitals. Other implementations of the MCDF method [14] make it possible to achieve convergence with much larger configuration sets. However full self-consistency is not achieved. Only selected subset of the configuration space are made self-consistent [15,16].

The shortcomings of our approach are thus compensated by the extra possibilities of our code. These shortcomings could lead to severe problems at low-Z, but at high-Z our method has been proven to be efficient and precise for simple systems (2 and 3-electron ions). To go beyond what we have achieved in the present work would require in our opinion to use a combination of MCDF and RMBPT. An other way would be to implement full support for non-orthogonal orbitals energy expression and a systematic method to build very large configuration space, but it is not clear at the moment that it would be sufficient to lead to more efficient and precise calculations at high-Z.

Our philosophy in this work was to put as many configurations as possible, limiting ourselves to principal quantum numbers in the range $1 \leq n \leq 3$ and trying to keep a balance between initial and final state correlation. This is particularly important since we included valence, core valence and core correlation. Core correlation would give a large effect on level energy, but would mostly cancel on transitions, and an imbalance in core correlation could shift the transition energy by a large amount.

The inclusion of a large amount of correlation in a relatively easy way, *i.e.*, with a small number of configurations, is an important feature of the MCDF method. It is also very good at picking up intra-shell correlation, a distinct advantage over RMBPT for Be-like or C-like ions, for example. The MCDF code that we use can also handle an arbitrary number of open shells. In our calculations we found many more transitions in the experimental window than reported in both experimental papers (41 *versus* 13). In order to see whether some of these transitions are contributing to the experimental spectrum, we have performed a complete calculation of transition rates, excitation (in the relativistic first Born approximation) and ionization cross sections.

In the few electron ions considered here, correlation is a sizable fraction of the transition energy. A combination of our MCDF code and a RMBPT code was used recently to calculate the energy of transitions between holes in singly ionized atoms [17,18] with good accuracy. In that process a good experience of comparing MCDF and RMBPT contributions was acquired. We use it here to make a detailed analysis of the transition energies in the F-like ions (considered here as a Ne-like ion with a $2p_{3/2}$ or a $2s_{1/2}$ hole), to access the quality of both calculations.

The paper is organized in the following way. In Section 2 we describe the MCDF method and our method for evaluating QED corrections. Then we describe the evaluation of transition rates and of ionization and excitation cross sections. In Section 3 we describe the RMBPT calculation of the F-like ion and make a detailed comparison with the MCDF and RCI results. We compare our results with the experiment in Section 4 and conclude in Section 5.

2 MCDF Calculation

2.1 Correlation

When dealing with the relativistic many-body problem, one has to combine many ingredients. A direct QED approach is currently unpractical for more than two electrons. It is thus customary to use either the MCDF method or the RMBPT to account for correlation, and correct this result for one and two-body QED contributions (self-energy, self-energy screening, ...). The correlation in this scheme is the sum of all the Feynman ladder diagrams. In this approach, non-radiative QED corrections to the electron-electron interaction cannot be easily incorporated, although they are of the same order of magnitude as radiative corrections to the electron-electron interaction. This comes from the fact that Hamiltonian methods are subject to the continuum dissolution problem [19,20] . To solve this problem one must use projection operators to avoid

an incorrect coupling of the $E > mc^2$ and the $E < -mc^2$ continua.

Projection operators had to be included from the beginning in RMBPT calculation, because if such a coupling between the $E > mc^2$ and the $E < -mc^2$ continua is allowed, it leads to infinite contributions (denominators cancel in second order perturbation terms). This was easily performed because all RMBPT calculations are done with finite basis set, and projection operators are implemented by limiting sums over intermediate states to $E > 0$ terms.

In the MCDF method in contrast, because the continua do not appear explicitly, projection operators have been implemented only recently [21]. The no-pair Hamiltonian is written [21–23]:

$$\mathcal{H}^{\text{nopair}} = \sum_{i=1}^{m} \mathcal{H}_{\text{D}}(r_i) + \sum_{i<j} \mathcal{V}\left(|\mathbf{r}_i - \mathbf{r}_j|\right), \tag{1}$$

where $\mathcal{H}_{\text{D}}$ is a one-electron Dirac operator and $\mathcal{V}$ is an operator representing the two-body interaction

$$\mathcal{V}_{ij} = \Lambda_{ij}^{++} V_{ij} \Lambda_{ij}^{++}. \tag{2}$$

In this equation we have, in the Coulomb Gauge,

$$V_{ij} = \frac{1}{r_{ij}} - \frac{\boldsymbol{\alpha}_i \cdot \boldsymbol{\alpha}_j}{r_{ij}} - \frac{\boldsymbol{\alpha}_i \cdot \boldsymbol{\alpha}_j}{r_{ij}} \left(\cos\left(\omega_{ij} r_{ij}\right) - 1\right) + \left(\boldsymbol{\alpha}_i \cdot \boldsymbol{\nabla}_i\right)\left(\boldsymbol{\alpha}_j \cdot \boldsymbol{\nabla}_j\right) \frac{\cos\left(\omega_{ij} r_{ij}\right) - 1}{\omega_{ij}^2 r_{ij}}, \tag{3}$$

where $r_{ij} = |\mathbf{r}_i - \mathbf{r}_j|$ is the inter-electronic distance, ω_{ij} is the energy of the photon exchanged between the electrons, $\boldsymbol{\alpha}_i$ are Dirac matrices ($\boldsymbol{\nabla}$ operators act on the r_{ij} and not on the the following wave function) and $\Lambda_{ij}^{++} = \Lambda_i^+ \Lambda_j^+$ is an operator projecting onto the one-electron positive energy states. However, there is no explicit expression for such an operator and other methods have to be found to include approximate projection operators in MCDF calculations [21].

The first term in equation (3) is the Coulomb interaction, the second one is the Gaunt (magnetic interaction) term and the other operators represent retardation (see, *e.g.*, [24,25]). The projection operators in equation (2) depend *a priori* on the one-electron potential chosen for the Hamiltonian [26,27] but it was checked in [21] that the final answer is very insensitive to the choice of potential, by using two variants of the Dirac-Fock potential.

2.2 Choice of configuration and of self-consistent potential

Although the MCDF method as described above, and as implemented in the code we used is completely general, there are several choices to be made to keep the calculation manageable. The first choice concerns the configuration set. Our current code is limited to $700jj$ configurations. For system with 2 to 5 electrons, this is usually sufficient. For more complex cases with several open shells, and in particular for the present calculation with a 2s hole in the initial state, the number of degenerated configurations issued from a single LS one can be very large. Here we had to limit ourselves with $n = 1$, 2 and 3 shells. Correlating hole states is also difficult in the MCDF method, because too many constraints are imposed to some orbitals. An orbital can be used at the same time as a regular, occupied orbital and as a correlation orbital for an inner shell. One should really have different labels for those orbitals (see, *e.g.*, [28]). However that would change the energy expression to account for non-orthogonality between orbitals of identical symmetry. Let's take an example. We want to do correlation on the 2s shell of $1s^2 2s^2 2p^2$. One possible candidate would be $1s^2 2p^4$. However in the 4 p electrons, 2 are real occupied orbitals, and 2 provide a correlation contribution to the $2s^2$ pair correlation. They will have a tendency to maximize their overlap with 2s, while the former have no reason to do so. So one should in reality add $1s^2 2p^2 2p'^2$. But then there should be extra terms in the energy expression involving the overlap $< 2p|2p' >$, which we do not know how to do at the present time, except for one electron operators evaluated between two different levels [29]. This will most likely lead to an underestimate of correlation energy. It also severely hampers convergence when too much constraints are set to a given orbital which is being used to correlate two orbitals in two very different region of space.

Several precautions must be taken when choosing configurations. In Table 1 we list the studied transitions and the upper and lower levels of each transition with the correspondent LS coupling labels (chosen to be the LS label of the component with largest weight). Additionally we included the number of LS and jj configurations used in the energy calculation of each level.

The LS configurations included as correlation in the calculation of the experimental observed transitions, except for neonlike, are displayed in Table 2 and Table 3.

2.3 Radiative corrections

Radiative corrections for many-electron atoms can be subdivided in two categories: one-electron corrections, which are identical to those of an hydrogenlike ion of the same nuclear charge, and two-electron effects, very often referred to as screening effects. In each case one has to evaluate a perturbation expansion in powers of the fine structure constant $\alpha \approx 1/137$, each power of α corresponding to one exchanged photon. There are also powers of $Z\alpha$ which represent the strength of the electron-nucleus interaction, which cannot be treated perturbatively at high-Z. The one-electron corrections start at order $\alpha(Z\alpha)^4\ mc^2$, while the two-electron ones start at order $\alpha^2(Z\alpha)^3\ mc^2$. The one-electron corrections of order $\alpha(Z\alpha)^4\ mc^2$ are composed of the self-energy and vacuum polarization terms. The self-energy part has been calculated for strong Coulomb fields by Mohr and collaborators [30–33] for several (n, ℓ), and must be corrected for finite nuclear size [34]. The vacuum polarization part can

Table 1. List of the studied transitions with LS coupling labels (chosen to be the LS label of the component with largest weight.) The LS and jj labels stands for the number of LS and jj configurations used, respectively.

Key	Upper level	LS	jj	Lower Level	LS	jj
Li	$(2p_{3/2})\ ^2P_{3/2}$	21	93	$(2s_{1/2})\ ^2S_{1/2}$	24	55
Be	$(2s_{1/2}\ 2p_{3/2})\ ^1P_1$	27	163	$(2s^2_{1/2})\ ^1S_0$	24	50
B1	$(2s_{1/2}\ 2p_{1/2}\ 2p_{3/2})\ ^2D_{3/2}$	13	37	$(2s^2_{1/2}\ 2p_{1/2})\ ^2P_{1/2}$	5	9
B2	$(2s_{1/2}\ 2p_{1/2}\ 2p_{3/2})\ ^2P_{1/2}$	13	33	$(2s^2_{1/2}\ 2p_{1/2})\ ^2P_{1/2}$	5	9
B3	$(2s_{1/2}\ 2p^2_{3/2})\ ^2S_{1/2}$	12	30	$(2s^2_{1/2}\ 2p_{3/2})\ ^2P_{3/2}$	11	42
B4	$(2s_{1/2}\ 2p^2_{3/2})\ ^2P_{3/2}$	10	34	$(2s^2_{1/2}\ 2p_{3/2})\ ^2P_{3/2}$	11	42
C1	$(2s_{1/2}\ 2p_{1/2}\ 2p^2_{3/2})\ ^3D_3$	10	62	$(2s^2_{1/2}\ 2p_{1/2}\ 2p_{3/2})\ ^1D_2$	13	60
C2	$(2s_{1/2}\ 2p^3_{3/2})\ ^3P_2$	13	91	$(2s^2_{1/2}\ 2p^2_{3/2})\ ^3P_2$	13	70
C3	$(2s_{1/2}\ 2p^3_{3/2})\ ^1P_1$	3	8	$(2s^2_{1/2}\ 2p^2_{3/2})\ ^1S_0$	4	8
C12	*ibid.*			$(2s^2_{1/2}\ 2p^2_{3/2})\ ^3P_2$	13	70
C4	$(2s_{1/2}\ 2p_{1/2}\ 2p^2_{3/2})\ ^3P_0$	14	36	$(2s^2_{1/2}\ 2p_{1/2}\ 2p_{3/2})\ ^3P_1$	14	56
C5	$(2s_{1/2}\ 2p^2_{1/2}\ 2p_{3/2})\ ^1P_1$	14	90	$(2s^2_{1/2}\ 2p^2_{1/2})\ ^3P_0$	15	32
C6	$(2s_{1/2}\ 2p_{1/2}\ 2p^2_{3/2})\ ^3S_1$	14	90	$(2s^2_{1/2}\ 2p_{1/2}\ 2p_{3/2})\ ^1D_2$	13	60
C9	*ibid.*			$(2s^2_{1/2}\ 2p_{1/2}\ 2p_{3/2})\ ^3P_1$	14	56
C7	$(2s_{1/2}\ 2p_{1/2}\ 2p^2_{3/2})\ ^1D_2$	14	92	$(2s^2_{1/2}\ 2p_{1/2}\ 2p_{3/2})\ ^1D_2$	13	60
C10	*ibid.*			$(2s^2_{1/2}\ 2p_{1/2}\ 2p_{3/2})\ ^3P_1$	14	56
C8	$(2s_{1/2}\ 2p_{1/2}\ 2p^2_{3/2})\ ^3P_1$	14	90	$(2s^2_{1/2}\ 2p_{1/2}\ 2p_{3/2})\ ^1D_2$	13	60
C11	*ibid.*			$(2s^2_{1/2}\ 2p_{1/2}\ 2p_{3/2})\ ^3P_1$	14	56
N1	$(2s_{1/2}\ 2p^2_{1/2}\ 2p^2_{3/2})\ ^4P_{5/2}$	10	129	$(2s^2_{1/2}\ 2p^2_{1/2}\ 2p_{3/2})\ ^2P_{3/2}$	12	62
N2	$(2s_{1/2}\ 2p_{1/2}\ 2p^3_{3/2})\ ^4P_{3/2}$	10	140	$(2s^2_{1/2}\ 2p_{1/2}\ 2p^2_{3/2})\ ^2D_{5/2}$	14	172
N3	*ibid.*			$(2s^2_{1/2}\ 2p_{1/2}\ 2p^2_{3/2})\ ^4S_{3/2}$	13	70
N4	$(2s_{1/2}\ 2p_{1/2}\ 2p^3_{3/2})\ ^2D_{5/2}$	10	129	$(2s^2_{1/2}\ 2p_{1/2}\ 2p^2_{3/2})\ ^2D_{5/2}$	14	172
N5	*ibid.*			$(2s^2_{1/2}\ 2p_{1/2}\ 2p^2_{3/2})\ ^4S_{3/2}$	13	70
N6	$(2s_{1/2}\ 2p_{1/2}\ 2p^3_{3/2})\ ^2P_{1/2}$	10	99	$(2s^2_{1/2}\ 2p_{1/2}\ 2p^2_{3/2})\ ^2P_{1/2}$	19	174
N12	*ibid.*			$(2s^2_{1/2}\ 2p_{1/2}\ 2p^2_{3/2})\ ^4S_{3/2}$	13	70
N7	$(2s_{1/2}\ 2p_{1/2}\ 2p^3_{3/2})\ ^2D_{3/2}$	10	140	$(2s^2_{1/2}\ 2p_{1/2}\ 2p^2_{3/2})\ ^2P_{1/2}$	19	174
N11	*ibid.*			$(2s^2_{1/2}\ 2p_{1/2}\ 2p^2_{3/2})\ ^2D_{5/2}$	14	172
N13	*ibid.*			$(2s^2_{1/2}\ 2p_{1/2}\ 2p^2_{3/2})\ ^4S_{3/2}$	13	70
N8	$(2s_{1/2}\ 2p^4_{3/2})\ ^4P_{1/2}$	4	8	$(2s^2_{1/2}\ 2p^3_{3/2})\ ^2P_{3/2}$	3	5
N9	$(2s_{1/2}\ 2p^2_{1/2}\ 2p^2_{3/2})\ ^2S_{1/2}$	12	152	$(2s^2_{1/2}\ 2p^2_{1/2}\ 2p_{3/2})\ ^2P_{3/2}$	12	62
N10	$(2s_{1/2}\ 2p^2_{1/2}\ 2p^2_{3/2})\ ^2P_{3/2}$	10	140	$(2s^2_{1/2}\ 2p^2_{1/2}\ 2p_{3/2})\ ^2P_{3/2}$	12	62
O1	$(2s_{1/2}\ 2p^2_{1/2}\ 2p^3_{3/2})\ ^3P_2$	18	226	$(2s^2_{1/2}\ 2p^2_{1/2}\ 2p^2_{3/2})\ ^3P_2$	20	419
O2	$(2s_{1/2}\ 2p_{1/2}\ 2p^4_{3/2})\ ^3P_0$	7[a]	55[a]	$(2s^2_{1/2}\ 2p_{1/2}\ 2p^3_{3/2})\ ^3P_1$	9[b]	56[b]
O3	$(2s_{1/2}\ 2p^2_{1/2}\ 2p^3_{3/2})\ ^1P_1$	18	226	$(2s^2_{1/2}\ 2p^2_{1/2}\ 2p^2_{3/2})\ ^1S_0$	20	419
O6	*ibid.*			$(2s^2_{1/2}\ 2p^2_{1/2}\ 2p^2_{3/2})\ ^3P_2$	20	419
O4	$(2s_{1/2}\ 2p_{1/2}\ 2p^4_{3/2})\ ^3P_1$	18[c]	226[c]	$(2s^2_{1/2}\ 2p_{1/2}\ 2p^3_{3/2})\ ^1D_2$	20[d]	419[d]
O5	*ibid.*			$(2s^2_{1/2}\ 2p_{1/2}\ 2p^3_{3/2})\ ^3P_1$	20	419
F	$(2s_{1/2}\ 2p^2_{1/2}\ 2p^4_{3/2})\ ^2S_{1/2}$	7	80	$(2s^2_{1/2}\ 2p^2_{1/2}\ 2p^3_{3/2})\ ^2P_{3/2}$	6	84
Ne1	$(2s_{1/2}\ 2p^2_{1/2}\ 2p^4_{3/2}\ 3s_{1/2})\ ^3S_1$	1	1	$(2s^2_{1/2}\ 2p^2_{1/2}\ 2p^3_{3/2}\ 3s_{1/2})\ ^1P_1$	8	170
Ne2	*ibid.*			$(2s^2_{1/2}\ 2p^2_{1/2}\ 2p^3_{3/2}\ 3s_{1/2})\ ^3P_2$	5	126
Ne3	$(2s_{1/2}\ 2p^2_{1/2}\ 2p^4_{3/2}\ 3s_{1/2})\ ^1S_0$	3	3	$(2s^2_{1/2}\ 2p^2_{1/2}\ 2p^3_{3/2}\ 3s_{1/2})\ ^1P_1$	8	170

[a] In the bismuth case we used 18 LS (82 jj Configurations).
[b] In the bismuth case we used 20 LS (327 jj Configurations).
[c] In the thorium case we used 7 LS (140 jj Configurations).
[d] In the thorium case we used 9 LS (75 jj Configurations).

Table 2. List of the LS configurations included as correlation in the calculation of the experimental observed transitions for lithiumlike, berylliumlike, boronlike and carbonlike.

Li		Be		B		C	
Initial	Final	Initial	Final	Initial	Final	Initial	Final
$2s^2\ 2p^1$	$1s^1\ 2s^2$	$1s^1\ 2s^2\ 2p^1$	$1s^2\ 2p^2$	$1s^1\ 2s^2\ 2p^2$	$1s^2\ 2p^3$	$1s^1\ 2p^5$	$1s^2\ 2p^4$
$2p^3$	$1s^1\ 2p^2$	$1s^1\ 2p^3$	$1s^2\ 3s^2$	$1s^1\ 2p^4$	$1s^1\ 2s^1\ 2p^3$	$2s^1\ 2p^5$	$1s^1\ 2s^1\ 2p^4$
$1s^2\ 3p^1$	$2s^1\ 2p^2$	$2s^1\ 2p^3$	$1s^2\ 3p^2$	$2s^1\ 2p^4$	$2s^2\ 2p^3$	$1s^2\ 2s^1\ 2p^2\ 3p^1$	$2s^2\ 2p^4$
$1s^1\ 2s^1\ 2p^1$	$2s^1\ 3s^2$	$1s^2\ 2s^1\ 3p^1$	$1s^2\ 3d^2$	$1s^2\ 2s^1\ 3s^2$	$2p^5$	$1s^2\ 2s^1\ 2p^1\ 3s^2$	$2p^6$
$1s^1\ 2s^1\ 3p^1$	$1s^1\ 2s^1\ 3s^1$	$1s^2\ 2p^1\ 3s^1$	$1s^2\ 2s^1\ 3s^1$	$1s^2\ 2s^1\ 2p^1\ 3p^1$		$1s^2\ 2s^1\ 2p^1\ 3p^2$	$1s^2\ 2s^2\ 2p^1\ 3p^1$
$1s^1\ 2p^1\ 3s^1$	$2s^2\ 3s^1$	$1s^2\ 2p^1\ 3d^1$	$1s^2\ 2s^1\ 3d^1$	$1s^2\ 2s^1\ 3s^1\ 3d^1$		$1s^2\ 2s^1\ 2p^1\ 3d^2$	$1s^2\ 2s^2\ 3s^2$
$1s^1\ 2p^1\ 3d^1$	$1s^1\ 2s^1\ 3p^1$	$1s^2\ 3s^1\ 3p^1$	$1s^2\ 2p^1\ 3p^1$	$1s^2\ 2s^1\ 3p^2$		$1s^2\ 2s^1\ 3s^2\ 3p^1$	$1s^2\ 2s^2\ 3s^1\ 3d^1$
$1s^1\ 3s^1\ 3p^1$	$2s^1\ 3p^2$	$1s^2\ 3p^1\ 3d^1$	$1s^2\ 3s^1\ 3d^1$	$1s^2\ 2s^1\ 3d^2$		$1s^2\ 2s^1\ 3p^1\ 3d^2$	$1s^2\ 2s^2\ 3p^2$
$1s^1\ 3p^1\ 3d^1$	$2s^1\ 3d^2$	$1s^1\ 2s^2\ 3p^1$	$1s^1\ 2s^2\ 3s^1$	$1s^2\ 2p^2\ 3s^1$		$1s^2\ 2s^1\ 3p^3$	$1s^2\ 2s^2\ 3d^2$
$2s^2\ 3p^1$	$1s^1\ 3s^2$	$1s^1\ 2s^1\ 2p^1\ 3s^1$	$1s^1\ 2s^2\ 3d^1$	$1s^2\ 3s^2\ 3d^1$		$1s^2\ 2s^2\ 2p^1\ 3s^1$	$1s^2\ 2s^1\ 2p^2\ 3s^1$
$2s^1\ 2p^1\ 3s^1$	$1s^1\ 3d^2$	$1s^1\ 2s^1\ 2p^1\ 3d^1$	$1s^1\ 2s^1\ 3s^2$	$1s^2\ 3s^1\ 3p^2$		$1s^2\ 2s^2\ 2p^1\ 3d^1$	$1s^2\ 2s^1\ 2p^2\ 3d^1$
$2s^1\ 2p^1\ 3d^1$	$1s^1\ 2s^1\ 3d^1$	$1s^1\ 2s^1\ 3s^1\ 3p^1$	$1s^1\ 2s^1\ 3d^2$	$1s^2\ 3s^1\ 3d^2$		$1s^2\ 2s^2\ 3s^1\ 3p^1$	$1s^2\ 2s^1\ 3s^2\ 3d^1$
$2s^1\ 3s^1\ 3p^1$	$1s^1\ 3p^2$	$1s^1\ 2s^1\ 3p^1\ 3d^1$	$1s^1\ 2s^1\ 3s^1\ 3d^1$			$1s^2\ 2s^2\ 3p^1\ 3d^1$	$1s^2\ 2s^1\ 3p^2\ 3d^1$
$2s^1\ 3p^1\ 3d^1$	$1s^2\ 3d^1$	$1s^1\ 2p^2\ 3p^1$	$1s^1\ 2s^1\ 2p^2$				$1s^2\ 2s^1\ 3d^3$
$2p^2\ 3p^1$	$2s^1\ 3s^1\ 3d^1$	$1s^1\ 2p^1\ 3s^2$	$1s^1\ 3s^1\ 3p^2$				
$2p^1\ 3s^2$	$2p^2\ 3s^1$	$1s^1\ 2p^1\ 3s^1\ 3d^1$	$1s^1\ 2s^1\ 3p^2$				
$2p^1\ 3p^2$	$2p^2\ 3d^1$	$1s^1\ 2p^1\ 3p^2$	$1s^1\ 2p^2\ 3s^1$				
$2p^1\ 3d^2$	$1s^2\ 3s^1$	$1s^1\ 2p^1\ 3d^2$	$1s^1\ 2p^2\ 3d^1$				
$3s^2\ 3p^1$	$3s^2\ 3d^1$	$1s^1\ 3s^2\ 3p^1$	$3s^2\ 3d^1$				
$3p^1\ 3d^2$	$3s^1\ 3p^2$	$1s^1\ 3s^1\ 3p^1\ 3d^1$	$1s^1\ 3s^1\ 3d^2$				
	$3s^1\ 3d^2$	$1s^1\ 3p^3$	$1s^1\ 3p^2\ 3d^1$				
	$3p^2\ 3d^1$	$1s^1\ 3p^1\ 3d^2$	$1s^1\ 3d^3$				
	$3d^3$	$2s^2\ 2p^1\ 3s^1$	$1s^1\ 2s^1\ 2p^1\ 3p^1$				
		$2s^2\ 2p^1\ 3d^1$					
		$2s^2\ 3s^1\ 3p^1$					
		$2s^2\ 3p^1\ 3d^1$					

be evaluated using well known potentials and can, in contrast to the self-energy, be calculated as a series expansion in $Z\alpha$. Here we include the first two contributions scaling as $\alpha(Z\alpha)^4\ mc^2$ (Uehling potential [35]) and as $\alpha(Z\alpha)^6\ mc^2$. All-order calculations have been performed and they show that the convergence in $Z\alpha$ is fast [36–38].

The second order one-electron radiative corrections have not been fully calculated. Still missing (for high-Z) is the two-loop self-energy (except for a piece of an irreducible diagram [39]), which can only be calculated by extrapolating recent calculations for low-Z [40]. This kind of extrapolation has been shown to be unreliable for the one loop self-energy [30], and we will use this value as an uncertainty in the theoretical calculation. For uranium all other pieces (mixed self-energy vacuum polarization diagrams [39,41]) have been calculated recently. The two-loop vacuum polarization can be easily calculated by combining the Källén and Sabry contribution [42], with the difference between self-consistent and perturbative calculations of the Uehling potential.

QED evaluations of two-electron contributions have been performed only for the two-electron ion case [43,44]. In most cases the calculation is done by evaluating one-electron self-energy in some screening potential [3,43,45–47]. Even those calculations are difficult and time consuming. In this paper we use an approximation based on the Welton method [9,48], which has been proven accurate by comparison with direct evaluation [49,47], although it cannot replace a *ab initio* calculation.

Finally, and to be complete, we include a nuclear polarization correction [50–52], which in this case is small compared to the experimental precision and second-order QED corrections.

In Table 4, an example of the energy calculation, for berylliumlike uranium, to show the typical order of magnitude of the different contributions described above. Energy values for all the 41 $2s_{1/2}-2p_{3/2}$ transitions that we have identified in the present calculation for uranium, thorium and bismuth are displayed in Tables 5, 6, and 7 respectively.

2.4 Relative intensities

Our calculation shows that there are many more lines in the experimental window than observed in the experiment. It was shown in both experiments that many lines are not produced because their initial state is not excited.

Table 3. List of the LS configurations included as correlation in the calculation of the experimental observed transitions for neonlike, oxygenlike and fluorinelike.

N		O		F	
Initial	Final	Initial	Final	Initial	Final
$1s^1\ 2s^2\ 2p^4$	$1s^2\ 2p^5$	$1s^1\ 2s^2\ 2p^5$	$1s^2\ 2p^6$	$1s^1\ 2s^2\ 2p^6$	$1s^2\ 2s^2\ 2p^4\ 3p^1$
$1s^1\ 2p^6$	$2s^2\ 2p^5$	$1s^2\ 2s^1\ 2p^4\ 3p^1$	$1s^1\ 2s^1\ 2p^6$	$1s^2\ 2s^1\ 2p^5\ 3p^1$	$1s^2\ 2s^2\ 2p^3\ 3s^2$
$2s^1\ 2p^6$	$1s^2\ 2s^2\ 2p^2\ 3p^1$	$1s^2\ 2s^1\ 2p^3\ 3s^2$	$2s^2\ 2p^6$	$1s^2\ 2s^1\ 2p^4\ 3s^2$	$1s^2\ 2s^2\ 2p^3\ 3s^1\ 3d^1$
$1s^2\ 2s^1\ 2p^3\ 3p^1$	$1s^2\ 2s^2\ 2p^1\ 3s^2$	$1s^2\ 2s^1\ 2p^3\ 3s^1\ 3d^1$	$1s^2\ 2s^2\ 2p^3\ 3p^1$	$1s^2\ 2s^1\ 2p^4\ 3s^1\ 3d^1$	$1s^2\ 2s^2\ 2p^3\ 3p^2$
$1s^2\ 2s^1\ 2p^2\ 3s^2$	$1s^2\ 2s^2\ 2p^1\ 3s^1\ 3d^1$	$1s^2\ 2s^1\ 2p^3\ 3p^2$	$1s^2\ 2s^2\ 2p^2\ 3s^2$	$1s^2\ 2s^1\ 2p^4\ 3p^2$	$1s^2\ 2s^2\ 2p^3\ 3d^2$
$1s^2\ 2s^1\ 2p^2\ 3p^2$	$1s^2\ 2s^2\ 2p^1\ 3p^2$	$1s^2\ 2s^1\ 2p^3\ 3d^2$	$1s^2\ 2s^2\ 2p^2\ 3s^1\ 3d^1$	$1s^2\ 2s^1\ 2p^4\ 3d^2$	
$1s^2\ 2s^1\ 2p^2\ 3s^1\ 3d^1$	$1s^2\ 2s^2\ 2p^1\ 3d^2$	$1s^2\ 2p^5\ 3s^1$	$1s^2\ 2s^2\ 2p^2\ 3p^2$		
$1s^2\ 2s^1\ 2p^2\ 3d^2$	$1s^2\ 2s^2\ 3s^2\ 3p^1$	$1s^2\ 2p^5\ 3d^1$	$1s^2\ 2s^2\ 2p^2\ 3d^2$		
$1s^2\ 2s^1\ 2p^1\ 3s^2\ 3p^1$	$1s^2\ 2s^2\ 3s^1\ 3p^1\ 3d^1$	$1s^1\ 2s^1\ 2p^5\ 3s^1$	$1s^1\ 2s^1\ 2p^4\ 3s^2$		
$1s^2\ 2s^1\ 2p^1\ 3s^1\ 3p^1\ 3d^1$	$1s^2\ 2s^2\ 3p^3$	$1s^1\ 2s^1\ 2p^5\ 3d^1$	$1s^1\ 2s^1\ 2p^4\ 3s^1\ 3d^1$		
$1s^2\ 2s^1\ 2p^1\ 3p^3$	$1s^2\ 2s^2\ 3p^1\ 3d^2$	$1s^1\ 2p^6\ 3p^1$	$1s^1\ 2s^1\ 2p^4\ 3p^2$		
		$2s^2\ 2p^5\ 3s^1$	$1s^1\ 2s^1\ 2p^4\ 3d^2$		
		$2s^2\ 2p^5\ 3d^1$	$1s^2\ 2p^4\ 3s^2$		
		$2s^1\ 2p^5\ 3s^2$	$1s^2\ 2p^4\ 3s^1\ 3d^1$		
		$2s^1\ 2p^5\ 3p^2$	$1s^2\ 2p^4\ 3p^2$		
		$2s^1\ 2p^5\ 3d^2$	$1s^2\ 2p^4\ 3d^2$		
		$2s^1\ 2p^6\ 3p^1$	$2s^2\ 2p^4\ 3s^2$		
			$2s^2\ 2p^4\ 3s^1\ 3d^1$		
			$2s^2\ 2p^4\ 3p^2$		
			$2s^2\ 2p^4\ 3d^2$		

Table 4. Contribution to the energy of the berylliumlike $(2s_{1/2}\ 2p_{3/2})^1P_1$ and $(2s^2_{1/2})^1S_0$ levels of U^{88+} and to the Be transition energy $E = (2s_{1/2}\ 2p_{3/2})^1P_1 - (2s^2_{1/2})^1S_0$. All energies are in eV.

	$(2s_{1/2}\ 2p_{3/2})\ ^1P_1$	$(2s^2_{1/2})\ ^1S_0$	E
Coulomb energy	−323068.194	−327614.170	4545.976
Magnetic energy	409.889	414.123	−4.234
Lowest-order order $(\Delta\omega^2)$	−14.896	−9.715	−5.182
High-order retardation $(\Delta\omega^n, n > 2)$	−5.603	1.271	−6.874
Electrostatic correlation	−1.159	−10.814	9.655
Magnetic correlation	−1.390	−2.256	0.866
Retardation correlation	0.296	0.335	−0.039
Self-energy	784.733	841.331	−56.598
Self-energy screening	−15.509	−18.657	3.149
Vacuum polarization (one loop)	−189.990	−204.673	14.683
Vacuum polarization (two loops)	−2.792	−3.037	0.245
Two loops SE + SE–VP			−0.110
Total level energy	−322104.615	−326606.262	4501.537

However not all transitions that we have found appear in the calculations carried out in [1–4]. We have thus tried to evaluate the relative intensities for all transitions. For that purpose we computed electron impact excitation and ionization cross sections as well as radiative transition rates and branching ratios for all identified transitions.

The transition rates are evaluated using our fully relativistic code [11,53], and taking into account non-orthogonality between initial and final states [12].

Electron-impact excitation cross sections were computed using the first Born approximation following the work of Kim *et al.* [54,55]. The electron beam energy was set to 100 keV as in the experiments reported in references [1,2]. In this calculation we used the MCDF wave functions for the atom and a Dirac wave function for the free electron. Only the Coulomb interaction between the free electron and the atomic electrons was considered.

Table 5. Effective excitation cross sections $\sigma^{\rm eff}_{\rm exc}$, effective ionization cross sections $\sigma^{\rm eff}_{\rm ion}$, effective cross sections $\sigma^{\rm eff} = \sigma^{\rm eff}_{\rm exc} + \sigma^{\rm eff}_{\rm ion}$, transition probabilities TP, branching ratios BR, relative intensities RI, and energies E of the $2s_{1/2} - 2p_{3/2}$ transitions in U^{89+} trough neonlike U^{82+} from our calculations. The excitation cross sections are in m^2, the transition probabilities are in s^{-1} and the energies are in eV. See Table 1 for definitions of Key.

Key	Ion	$\sigma^{\rm eff}_{\rm exc}$	$\sigma^{\rm eff}_{\rm ion}$	$\sigma^{\rm eff}$	TP	BR	RI	E
Li	U^{89+}	1.80×10^{-26}	0.00	1.80×10^{-26}	8.53×10^{13}	1.00	0.67	4460.00
Be	U^{88+}	1.85×10^{-26}	0.00	1.85×10^{-26}	1.20×10^{14}	1.00	0.69	4501.54
B1	U^{87+}	2.40×10^{-26}	0.00	2.40×10^{-26}	1.20×10^{14}	1.00	0.89	4522.09
B2	U^{87+}	1.26×10^{-26}	0.00	1.26×10^{-26}	1.25×10^{14}	1.00	0.47	4522.37
B3	U^{87+}	9.71×10^{-31}	0.00	9.71×10^{-31}	9.34×10^{13}	1.00	0.00	4540.66
B4	U^{87+}	2.55×10^{-30}	0.00	2.55×10^{-30}	1.86×10^{14}	1.00	0.00	4542.40
C1	U^{86+}	0.00	2.11×10^{-27}	2.11×10^{-27}	2.90×10^{13}	1.00	0.08	4426.33
C2	U^{86+}	0.00	1.51×10^{-27}	1.51×10^{-27}	9.11×10^{13}	1.00	0.06	4478.65
C3	U^{86+}	2.53×10^{-36}	9.04×10^{-28}	9.04×10^{-28}	6.15×10^{13}	0.28	0.01	4501.29
C4	U^{86+}	0.00	3.01×10^{-28}	3.01×10^{-28}	9.27×10^{13}	1.00	0.01	4540.65
C5	U^{86+}	1.83×10^{-26}	9.04×10^{-28}	1.92×10^{-26}	1.24×10^{14}	1.00	0.72	4550.56
C6	U^{86+}	2.27×10^{-30}	9.04×10^{-28}	9.06×10^{-28}	2.00×10^{13}	0.11	0.00	4555.61
C7	U^{86+}	0.00	1.51×10^{-27}	1.51×10^{-27}	1.73×10^{14}	0.92	0.05	4560.57
C8	U^{86+}	1.48×10^{-30}	9.04×10^{-28}	9.05×10^{-28}	9.36×10^{13}	0.95	0.03	4566.43
C9	U^{86+}	2.27×10^{-30}	9.04×10^{-28}	9.06×10^{-28}	1.69×10^{14}	0.89	0.03	4572.28
C10	U^{86+}	0.00	1.51×10^{-27}	1.51×10^{-27}	1.41×10^{13}	0.08	0.00	4577.24
C11	U^{86+}	1.48×10^{-30}	9.04×10^{-28}	9.05×10^{-28}	4.67×10^{12}	0.05	0.00	4583.10
C12	U^{86+}	2.53×10^{-36}	9.04×10^{-28}	9.04×10^{-28}	1.62×10^{14}	0.72	0.02	4600.16
N1	U^{85+}	9.49×10^{-27}	2.41×10^{-27}	1.19×10^{-26}	2.97×10^{13}	1.00	0.44	4440.57
N2	U^{85+}	1.97×10^{-30}	1.61×10^{-27}	1.61×10^{-27}	3.01×10^{12}	0.03	0.00	4464.37
N3	U^{85+}	1.97×10^{-30}	1.61×10^{-27}	1.61×10^{-27}	8.98×10^{13}	0.97	0.06	4483.04
N4	U^{85+}	2.38×10^{-31}	2.41×10^{-27}	2.41×10^{-27}	8.71×10^{13}	0.94	0.08	4508.48
N5	U^{85+}	2.38×10^{-31}	8.03×10^{-28}	8.04×10^{-28}	5.93×10^{12}	0.06	0.00	4527.16
N6	U^{85+}	8.73×10^{-31}	1.61×10^{-27}	1.61×10^{-27}	6.41×10^{13}	0.28	0.02	4531.10
N7	U^{85+}	4.76×10^{-30}	8.03×10^{-28}	8.08×10^{-28}	6.12×10^{13}	0.27	0.01	4534.97
N8	U^{85+}	8.09×10^{-37}	8.03×10^{-28}	8.03×10^{-28}	1.91×10^{14}	1.00	0.03	4548.77
N9	U^{85+}	9.21×10^{-27}	1.61×10^{-27}	1.08×10^{-26}	9.68×10^{13}	1.00	0.40	4586.94
N10	U^{85+}	3.66×10^{-26}	2.41×10^{-27}	3.90×10^{-26}	1.93×10^{14}	0.69	1.00	4589.58
N11	U^{85+}	4.76×10^{-30}	1.61×10^{-27}	1.61×10^{-27}	1.57×10^{14}	0.69	0.04	4612.96
N12	U^{85+}	8.73×10^{-31}	8.03×10^{-28}	8.04×10^{-28}	1.64×10^{14}	0.72	0.02	4627.77
N13	U^{85+}	4.76×10^{-30}	1.61×10^{-27}	1.61×10^{-27}	8.09×10^{12}	0.04	0.00	4631.64
O1	U^{84+}	2.35×10^{-26}	2.91×10^{-27}	2.64×10^{-26}	1.57×10^{14}	1.00	0.98	4526.10
O2	U^{84+}	0.00	5.82×10^{-28}	5.82×10^{-28}	3.79×10^{13}	1.00	0.02	4527.88
O3	U^{84+}	2.28×10^{-26}	1.75×10^{-27}	2.46×10^{-26}	6.37×10^{13}	0.50	0.45	4558.49
O4	U^{84+}	2.95×10^{-30}	1.75×10^{-27}	1.75×10^{-27}	1.65×10^{14}	0.84	0.05	4572.68
O5	U^{84+}	2.95×10^{-30}	1.75×10^{-27}	1.75×10^{-27}	3.17×10^{13}	0.16	0.01	4573.49
O6	U^{84+}	2.28×10^{-26}	1.75×10^{-27}	2.46×10^{-26}	2.00×10^{11}	0.50	0.46	4643.12
F	U^{83+}	1.87×10^{-26}	1.16×10^{-27}	1.98×10^{-26}	1.98×10^{14}	1.00	0.74	4594.83
Ne1	U^{82+}	0.00	3.93×10^{-27}	3.93×10^{-27}	3.29×10^{13}	0.17	0.02	4583.93
Ne2	U^{82+}	0.00	3.93×10^{-27}	3.93×10^{-27}	1.65×10^{14}	0.83	0.12	4595.80
Ne3	U^{82+}	1.19×10^{-26}	1.31×10^{-27}	1.32×10^{-26}	2.10×10^{14}	1.00	0.49	4635.07

Table 6. Effective excitation cross sections $\sigma^{\rm eff}_{\rm exc}$, effective ionization cross sections $\sigma^{\rm eff}_{\rm ion}$, effective cross sections $\sigma^{\rm eff} = \sigma^{\rm eff}_{\rm exc} + \sigma^{\rm eff}_{\rm ion}$, transition probabilities TP, branching ratios BR, relative intensities RI, and energies E of the $2s_{1/2} - 2p_{3/2}$ transitions in Th^{87+} trough neonlike Th^{80+} from our calculations. The excitation cross sections are in m^2, the transition probabilities are in s^{-1} and the energies are in eV. See Table 1 for definitions of Key.

Key	Ion	$\sigma^{\rm eff}_{\rm exc}$	$\sigma^{\rm eff}_{\rm ion}$	$\sigma^{\rm eff}$	TP	BR	RI	E
Li	Th^{87+}	1.97×10^{-26}	0.00	1.97×10^{-26}	6.63×10^{13}	1.00	0.67	4025.85
Be	Th^{86+}	2.02×10^{-26}	0.00	2.02×10^{-26}	9.38×10^{13}	1.00	0.69	4068.21
B1	Th^{85+}	2.62×10^{-26}	0.00	2.62×10^{-26}	9.37×10^{13}	1.00	0.89	4090.92
B2	Th^{85+}	1.38×10^{-26}	0.00	1.38×10^{-26}	9.84×10^{13}	1.00	0.47	4090.76
B3	Th^{85+}	1.24×10^{-30}	0.00	1.24×10^{-30}	7.34×10^{13}	1.00	0.00	4108.09
B4	Th^{85+}	3.30×10^{-30}	0.00	3.30×10^{-30}	1.46×10^{14}	1.00	0.00	4109.79
C1	Th^{84+}	0.00	2.55×10^{-27}	2.55×10^{-27}	2.27×10^{13}	1.00	0.09	3999.57
C2	Th^{84+}	0.00	1.82×10^{-27}	1.82×10^{-27}	7.15×10^{13}	1.00	0.06	4049.14
C3	Th^{84+}	2.49×10^{-36}	1.09×10^{-27}	1.09×10^{-27}	4.83×10^{13}	0.27	0.01	4071.31
C4	Th^{84+}	0.00	3.64×10^{-28}	3.64×10^{-28}	7.28×10^{13}	1.00	0.01	4109.66
C5	Th^{84+}	2.00×10^{-26}	1.09×10^{-27}	2.11×10^{-26}	9.78×10^{13}	1.00	0.71	4120.07
C6	Th^{84+}	2.93×10^{-30}	1.09×10^{-27}	1.09×10^{-27}	1.57×10^{13}	0.11	0.00	4123.36
C7	Th^{84+}	0.00	1.82×10^{-27}	1.82×10^{-27}	1.36×10^{14}	0.93	0.06	4128.98
C8	Th^{84+}	1.91×10^{-30}	1.09×10^{-27}	1.09×10^{-27}	7.40×10^{13}	0.95	0.04	4134.57
C9	Th^{84+}	2.93×10^{-30}	1.09×10^{-27}	1.09×10^{-27}	1.33×10^{14}	0.89	0.03	4140.49
C10	Th^{84+}	0.00	1.82×10^{-27}	1.82×10^{-27}	1.10×10^{13}	0.07	0.00	4146.11
C11	Th^{84+}	1.91×10^{-30}	1.09×10^{-27}	1.09×10^{-27}	3.54×10^{12}	0.05	0.00	4151.70
C12	Th^{84+}	2.49×10^{-36}	1.09×10^{-27}	1.09×10^{-27}	1.27×10^{14}	0.73	0.03	4172.44
N1	Th^{83+}	1.04×10^{-26}	2.91×10^{-27}	1.33×10^{-26}	2.33×10^{13}	1.00	0.45	4016.29
N2	Th^{83+}	2.56×10^{-30}	1.94×10^{-27}	1.94×10^{-27}	2.35×10^{12}	0.03	0.00	4037.19
N3	Th^{83+}	2.56×10^{-30}	1.94×10^{-27}	1.94×10^{-27}	7.06×10^{13}	0.97	0.06	4056.41
N4	Th^{83+}	3.00×10^{-31}	2.91×10^{-27}	2.91×10^{-27}	6.85×10^{13}	0.94	0.09	4081.42
N5	Th^{83+}	3.00×10^{-31}	9.70×10^{-28}	9.70×10^{-28}	4.65×10^{12}	0.06	0.00	4100.64
N6	Th^{83+}	1.14×10^{-30}	1.94×10^{-27}	1.94×10^{-27}	5.06×10^{13}	0.28	0.02	4102.73
N7	Th^{83+}	6.15×10^{-30}	9.70×10^{-28}	9.76×10^{-28}	4.81×10^{13}	0.27	0.01	4107.22
N8	Th^{83+}	2.51×10^{-36}	9.70×10^{-28}	9.70×10^{-28}	1.51×10^{14}	1.00	0.03	4119.59
N9	Th^{83+}	1.00×10^{-26}	1.94×10^{-27}	1.20×10^{-26}	7.63×10^{13}	1.00	0.41	4157.77
N10	Th^{83+}	3.99×10^{-26}	2.91×10^{-27}	4.28×10^{-26}	1.52×10^{14}	0.69	1.00	4160.34
N11	Th^{83+}	6.15×10^{-30}	1.94×10^{-27}	1.95×10^{-27}	1.24×10^{14}	0.69	0.05	4182.05
N12	Th^{83+}	1.14×10^{-30}	9.70×10^{-28}	9.71×10^{-28}	1.29×10^{14}	0.72	0.02	4196.79
N13	Th^{83+}	6.15×10^{-30}	1.94×10^{-27}	1.95×10^{-27}	6.30×10^{12}	0.04	0.00	4201.27
O1	Th^{82+}	2.57×10^{-26}	3.23×10^{-27}	2.89×10^{-26}	1.24×10^{14}	1.00	0.98	4100.77
O2	Th^{82+}	0.00	6.47×10^{-28}	6.47×10^{-28}	2.99×10^{13}	1.00	0.02	4119.40
O3	Th^{82+}	2.49×10^{-26}	1.94×10^{-27}	2.68×10^{-26}	5.03×10^{13}	0.50	0.45	4132.11
O4	Th^{82+}	3.83×10^{-30}	1.94×10^{-27}	1.94×10^{-27}	1.30×10^{14}	0.84	0.06	4145.01
O5	Th^{82+}	3.83×10^{-30}	1.94×10^{-27}	1.94×10^{-27}	2.50×10^{13}	0.16	0.01	4162.59
O6	Th^{82+}	2.49×10^{-26}	1.94×10^{-27}	2.68×10^{-26}	1.91×10^{11}	0.50	0.46	4213.79
F	Th^{81+}	2.03×10^{-26}	1.29×10^{-27}	2.16×10^{-26}	1.57×10^{14}	1.00	0.73	4169.05
Ne1	Th^{80+}	0.00	4.37×10^{-27}	4.37×10^{-27}	2.61×10^{13}	0.17	0.02	4159.35
Ne2	Th^{80+}	0.00	4.37×10^{-27}	4.37×10^{-27}	1.31×10^{14}	0.83	0.12	4170.82
Ne3	Th^{80+}	1.35×10^{-26}	1.46×10^{-27}	1.50×10^{-26}	1.66×10^{14}	1.00	0.51	4207.82

Table 7. Effective excitation cross sections $\sigma^{\rm eff}_{\rm exc}$, effective ionization cross sections $\sigma^{\rm eff}_{\rm ion}$, effective cross sections $\sigma^{\rm eff} = \sigma^{\rm eff}_{\rm exc} + \sigma^{\rm eff}_{\rm ion}$, transition probabilities TP, branching ratios BR, relative intensities RI, and energies E of the $2s_{1/2} - 2p_{3/2}$ transitions in Bi^{80+} trough neonlike Bi^{73+} from our calculations. The excitation cross sections are in m^2, the transition probabilities are in s^{-1} and the energies are in eV. See Table 1 for definitions of Key.

Key	Ion	$\sigma^{\rm eff}_{\rm exc}$	$\sigma^{\rm eff}_{\rm ion}$	$\sigma^{\rm eff}$	TP	BR	RI	E
Li	Bi^{80+}	2.67×10^{-26}	0.00	2.67×10^{-26}	2.70×10^{13}	1.00	0.67	2788.47
Be	Bi^{79+}	2.76×10^{-26}	0.00	2.76×10^{-26}	3.90×10^{13}	1.00	0.69	2833.04
B1	Bi^{78+}	3.55×10^{-26}	0.00	3.55×10^{-26}	3.92×10^{13}	1.00	0.88	2860.13
B2	Bi^{78+}	1.89×10^{-26}	0.00	1.89×10^{-26}	4.16×10^{13}	1.00	0.47	2858.80
B3	Bi^{78+}	2.95×10^{-30}	0.00	2.95×10^{-30}	3.10×10^{13}	1.00	0.00	2873.57
B4	Bi^{78+}	8.25×10^{-30}	0.00	8.25×10^{-30}	6.15×10^{13}	1.00	0.00	2875.22
C1	Bi^{77+}	0.00	3.66×10^{-27}	3.66×10^{-27}	9.46×10^{12}	1.00	0.09	2784.89
C2	Bi^{77+}	0.00	2.61×10^{-27}	2.61×10^{-27}	3.02×10^{13}	1.00	0.07	2826.64
C3	Bi^{77+}	1.05×10^{-35}	1.57×10^{-27}	1.57×10^{-27}	2.04×10^{13}	0.27	0.01	2861.73
C4	Bi^{77+}	0.00	5.23×10^{-28}	5.23×10^{-28}	3.08×10^{13}	1.00	0.01	2881.21
C5	Bi^{77+}	2.71×10^{-26}	1.57×10^{-27}	2.86×10^{-26}	4.14×10^{13}	1.00	0.71	2892.39
C6	Bi^{77+}	7.20×10^{-30}	1.57×10^{-27}	1.57×10^{-27}	6.30×10^{12}	0.10	0.00	2891.08
C7	Bi^{77+}	0.00	2.61×10^{-27}	2.61×10^{-27}	5.79×10^{13}	0.93	0.06	2898.65
C8	Bi^{77+}	4.84×10^{-30}	1.57×10^{-27}	1.57×10^{-27}	3.22×10^{13}	0.96	0.04	2903.25
C9	Bi^{77+}	7.20×10^{-30}	1.57×10^{-27}	1.57×10^{-27}	5.71×10^{13}	0.90	0.04	2909.16
C10	Bi^{77+}	0.00	2.61×10^{-27}	2.61×10^{-27}	4.59×10^{12}	0.07	0.00	2916.73
C11	Bi^{77+}	4.84×10^{-30}	1.57×10^{-27}	1.57×10^{-27}	1.19×10^{12}	0.04	0.00	2921.33
C12	Bi^{77+}	1.05×10^{-35}	1.57×10^{-27}	1.57×10^{-27}	5.45×10^{13}	0.73	0.03	2946.45
N1	Bi^{76+}	1.42×10^{-26}	4.18×10^{-27}	1.83×10^{-26}	9.81×10^{12}	1.00	0.46	2805.32
N2	Bi^{76+}	6.51×10^{-30}	2.79×10^{-27}	2.79×10^{-27}	9.84×10^{11}	0.03	0.00	2818.27
N3	Bi^{76+}	6.51×10^{-30}	2.79×10^{-27}	2.79×10^{-27}	3.00×10^{13}	0.97	0.07	2838.80
N4	Bi^{76+}	6.82×10^{-31}	4.18×10^{-27}	4.18×10^{-27}	2.92×10^{13}	0.94	0.10	2862.12
N5	Bi^{76+}	6.82×10^{-31}	1.39×10^{-27}	1.39×10^{-27}	1.95×10^{12}	0.06	0.00	2882.65
N6	Bi^{76+}	2.92×10^{-30}	2.79×10^{-27}	2.79×10^{-27}	2.17×10^{13}	0.28	0.02	2879.41
N7	Bi^{76+}	1.52×10^{-29}	1.39×10^{-27}	1.41×10^{-27}	2.04×10^{13}	0.27	0.01	2885.83
N8	Bi^{76+}	4.30×10^{-35}	1.39×10^{-27}	1.39×10^{-27}	6.47×10^{13}	1.00	0.03	2894.43
N9	Bi^{76+}	1.36×10^{-26}	2.79×10^{-27}	1.64×10^{-26}	3.28×10^{13}	1.00	0.41	2930.60
N10	Bi^{76+}	5.39×10^{-26}	4.18×10^{-27}	5.81×10^{-26}	6.51×10^{13}	0.69	1.00	2933.07
N11	Bi^{76+}	1.52×10^{-29}	2.79×10^{-27}	2.80×10^{-27}	5.37×10^{13}	0.70	0.05	2950.33
N12	Bi^{76+}	2.92×10^{-30}	1.39×10^{-27}	1.40×10^{-27}	5.57×10^{13}	0.72	0.03	2964.44
N13	Bi^{76+}	1.52×10^{-29}	2.79×10^{-27}	2.80×10^{-27}	2.59×10^{12}	0.03	0.00	2970.86
O1	Bi^{75+}	3.49×10^{-26}	4.64×10^{-27}	3.95×10^{-26}	5.33×10^{13}	1.00	0.99	2885.41
O2	Bi^{75+}	0.00	9.29×10^{-28}	9.29×10^{-28}	1.28×10^{13}	1.00	0.02	2899.16
O3	Bi^{75+}	3.36×10^{-26}	2.79×10^{-27}	3.64×10^{-26}	2.16×10^{13}	0.49	0.45	2913.40
O4	Bi^{75+}	9.68×10^{-30}	2.79×10^{-27}	2.80×10^{-27}	5.67×10^{13}	0.84	0.06	2921.66
O5	Bi^{75+}	9.68×10^{-30}	2.79×10^{-27}	2.80×10^{-27}	1.07×10^{13}	0.16	0.01	2940.23
O6	Bi^{75+}	3.36×10^{-26}	2.79×10^{-27}	3.64×10^{-26}	1.59×10^{11}	0.51	0.46	2985.24
F	Bi^{74+}	2.76×10^{-26}	1.86×10^{-27}	2.94×10^{-26}	6.83×10^{13}	1.00	0.73	2951.07
Ne1	Bi^{73+}	0.00	6.27×10^{-27}	6.27×10^{-27}	1.14×10^{13}	0.17	0.03	2943.73
Ne2	Bi^{73+}	0.00	6.27×10^{-27}	6.27×10^{-27}	5.71×10^{13}	0.83	0.13	2956.99
Ne3	Bi^{73+}	2.20×10^{-26}	2.09×10^{-27}	2.41×10^{-26}	7.28×10^{13}	1.00	0.60	2986.15

Table 8. Detailed breakdown of the contributions to the transition energy between $1s^2 2s 2p_{1/2}^2 2p_{3/2}^4$ and $1s^2 2s^2 2p_{1/2}^2 2p_{3/2}^3$ in F-like uranium. All individual corrections include effects due to the finite size of the nucleus and the reduced mass of the electron.

		MBPT		MCDF	CI [a]
Coulomb					
frozen core		4642.571		4642.571	
2nd order contributions	relaxation	−0.127		−0.049 [b]	
	core-core	−1.590			
	correlation	−0.859			
higher order	relaxation	0.007			
	core-core	−0.017			
	Total corr.+cc		−2.459	−1.732	
Total		4639.985		4640.790	4640.230
Breit					
frozen core		−1.614 [c]		−1.759 [d]	
2nd order contributions	relaxation	−0.018		−0.066	
	core-core	−0.192			
	correlation	−0.032			
	Total corr.+cc		−0.224	−0.392	
Retardation beyond Breit					
frozen core		−6.378		−6.378	
2nd order contributions					
	relaxation	−0.093		−0.093	
	correlation	0.032		0.032	
Total		−8.295		−8.656	−8.500
Mass polarization		−0.040		−0.040	−0.040
Total many-body part		4631.650		4632.094	4631.690
QED					
Self-energy (one loop)	one electron			−56.598	
	two-electron			5.151	
Vacuum Polarization (one loop)					
Uehling	one electron			16.336	
	two-electron			−1.557	
Wichman and Kroll	one-electron			−0.739	
	two-electron			0.064	
Self-energy (two loops)				0.080(80)	
Vacuum pol.(two loops)				0.155	
Mixed SE-VP				−0.190	
Total QED				−37.297	−38.020
Nuclear Polarization [50–52]		0.030		0.030	0.030
Total		4594.383		4594.827	4593.700
Experiment		4593.83(12)			
Exp.-Theory		−0.553		−0.997	0.130

[a] Cheng and Chen [3].
[b] The MCDF results are not strict 2nd order effects, but includes higher orders as well.
[c] Obtained with the Breit interaction treated self-consistently as a Dirac-Fock-Breit potential.
[d] Obtained with the Gaunt interaction treated self-consistently as a Dirac-Fock-Gaunt potential.

Because of the high electron beam energy in the EBIT the first Born approximation is adequate.

A full evaluation of the ionization cross-section would be a daunting task. Recently a new method was reported by Kim and Rudd [56], which has been shown to provide accurate results, even at energies close to the ionization threshold. Here we use the approximation in which only the binding energy of the ionized electron and the kinetic energy of the incoming electron are needed. The population of the different J sublevels of the final state is assumed to be statistical.

The relative intensity for each spectral line was evaluated by multiplying the sum of the corresponding ionization and excitation cross sections for all possible ground states leading to the initial state of the transition, by the branching ratio. The results were normalized to the maximum intensity obtained over all ionic species for a given ion. As in the experimental paper, we assume that all ionic species present in the EBIT have equal intensities, and that all ions are in their ground state (low collisionality hypothesis). We also neglected cascade from higher-lying excited states, because of the complexity of such a

calculation, which would necessitate a complete modeling of the EBIT, a task well beyond the scope of the present paper.

The results of these calculations are displayed in Tables 5, 6, and 7 for the three ions studied here. We find that the prominent lines correspond to those identified in the two experimental papers.

3 Detailed comparison between RMBPT and MCDF for F-like uranium

In the last few years [17,57] two of us have successfully combined MCDF and RMBPT for transitions between hole states in heavy elements. Generally we have treated singly charged systems, which can be viewed as the neutral element plus a hole. $K\alpha$ - transitions in uranium were, *e.g.*, treated in this way. Fluorine-like systems can be viewed as a neon-like system with a hole and we have thus a very similar situation to the singly charged hole states, although the complications due to the 82 electrons with $n > 2$, in the case of uranium, is removed.

For inner hole states the correlation contribution is not dominated by the admixture of a few important configurations, instead it is the sum of many contributions each with a rather low weight. Due to the large nuclear charge felt by the inner electrons the correlation is also dominated by second order effects. This is an ideal situation for RMBPT, which consequently is a convenient choice for calculating correlation is these systems.

As a starting point for fluorine-like uranium we choose the neon-like system and perturb it with either a hole in 2s or a hole in $2p_{3/2}$. The lowest order contributions to the shift due to a hole is the opposite of the eigenvalue of the Dirac-Fock Hamiltonian. This is the frozen core result on the first row of Table 8. It is called frozen since the other core orbitals have not had the possibility to relax due to the presence of the hole. This relaxation is then calculated separately. For general hole states this is a very important contribution. In reference [17], *e.g.*, it was found to be -37.8 eV for a 2s-hole in xenon and an accurate calculation requires then relaxation effects to all orders. However, for fluorine-like uranium the relaxation is much less important, ≈ -3 eV and the cancellation between a 2s and a $2p_{3/2}$ hole is almost perfect, probably due to the absence of $n > 2$-electrons. A treatment to second order is thus sufficient, which can be seen from the small effect from higher order relaxation in Table 8. In an MCDF calculation the relaxation is included when the single configuration result is calculated in a spherical-symmetric Hartree-Fock potential including the hole. The relaxation obtained with the two approaches differs slightly since the RMBPT result includes also effects which cannot be accounted for by a spherical-symmetric potential. Usually these latter effects are, however, of minor importance. In Table 8 small, but quite different, relaxation contributions are found with RMBPT and MCDF. The relatively big difference is probably due to the large cancellation between the relaxation for a 2s and a $2p_{3/2}$ hole, which exposes small differences. On the next rows in Table 8 we list more detailed many-body effects. By correlation we mean admixture of configurations consisting of two excited orbitals. A discrete numerical basis set is used to describe the bound states and the continuum as described in [17,57–59]. We also include admixture of configurations where the hole in, *e.g.*, 2s, is replaced by two holes in other orbitals and one electron in an excited orbital. This effect, called core-core contribution, contributes by -1.59 eV. This effect is also treated to all orders, where it is allowed to mix with relaxation contributions, and a small contribution of ≈ -0.02 eV is then obtained. In these admixtures we include excited orbitals with $\ell_{\max} = 10$ ($\ell_{\max} = 6$ for Breit contributions which will be discussed below). In the MCDF calculation the correlation and core-core contributions are calculated together. Configurations including orbitals up to $3d_{5/2}$ are included and the result is -1.67 eV which should be compared to $-1.59 - 0.86 = -2.45$ eV from the RMBPT calculation. The difference is most likely due to the smaller number of excited configurations included in the MCDF calculation. The MCDF calculation does also include some contributions not accounted for by perturbation theory corresponding to triple and quadruple excitations, but we have no measure of how important these are.

The next step is to add the Breit interaction and calculate how the different contributions change. The results are displayed in Table 8. In the RMBPT calculation the Breit interaction is included in the orbitals which are obtained self-consistently in the Dirac-Fock-Breit potential. The MCDF calculation treats only the Gaunt part (*i.e.*, the magnetic part) of the Breit interaction in this way, which might explain the difference in the frozen core and relaxation results. The difference in the Breit correlation is explained, as for the Coulomb correlation, by the number of included configurations.

When different calculation schemes are compared it is important to compare them at the lowest possible level, otherwise it is very hard to understand how the differences appear. All calculations of transitions in heavy ions consist of one many-body part and one part due to radiative effects, usually called QED. In Table 9 we compare our RMBPT calculation with the MBPT calculations by Johnson *et al.* [4]. In perturbation theory it is possible to use different starting potentials. The final result should be independent of the starting point provided the perturbation expansion is carried on to all orders. In practice one has always, except perhaps for very small systems, to introduce approximations. The many-body effects included in both calculations are, *e.g.*, limited to the so called single and double excitations and reference [4] is strictly restricted to second order contributions. Finally both calculations neglect correlation contributions from virtual electron-positron pairs, which in principle are needed if a calculation should be independent of the starting point. Small differences due to the starting point are thus expected. In reference [4] two different local potentials are used. One is the direct part of the Dirac-Fock potential from a neon-like core (called potential A). The other potential, called potential B, is also the direct part of the

Table 9. A comparison between the many-body effects for the transition energy between $1s^2 2s 2p_{1/2}^2 2p_{3/2}^4$ and $1s^2 2s^2 2p_{1/2}^2 2p_{3/2}^3$ in F-like uranium as calculated here and in reference [4]. Both calculations use relativistic many-body perturbation theory and the results are displayed on different levels in the perturbation expansion. The lowest and first order results include Coulomb and Breit interaction as well as retardation beyond Breit interaction and effects due to the finite mass and size of the nucleus. The starting potential is here the Dirac-Fock-Breit potential for the closed shell neon-like system, while potential A and B from reference [4] refer to two different local potentials. The result from an all order treatment should be independent of the starting potential and the difference between the different starting points is an indication of the importance of higher order effects.

	Present	reference [4] potential A	reference [4] potential B
lowest and first order	4634.447	4633.459	4633.603
Coulomb 2nd order	−2.576	−1.859	−1.899
Breit 2nd order	−0.241	0.016	−0.139
Coulomb higher order	−0.010		
MBPT	4631.619	4631.616	4631.565
QED		−37.304	−37.549

Dirac-Fock potential, but for one $2p_{3/2}$-electron less. In the present calculation we use the full Dirac-Fock-Breit potential for the neon-like system. The difference relative to the result obtained with potential A of reference [4] is the exchange contribution and the Breit interaction. Although the contributions on different levels in the perturbation expansion are quite different, due to different starting points (see Tab. 9), the final MBPT results are very similar with all three approaches. We note especially that the present result and the result from potential A of reference [4] agree well within 0.01 eV. The good agreement between the three starting points as well as the small size of the calculated higher terms from the perturbation expansion indicate that the system is indeed dominated by effects up to second order in the expansion.

In Table 8 we compare our results with the CI calculation by Cheng and Chen [3]. The starting point in reference [3] is a Dirac-Slater potential with an approximation of the exchange contribution included. The calculation includes the so called singles and doubles, which is the same as in the MBPT calculations. The inclusion of excited configurations is truncated after $\ell_{\max} = 3$, and the contributions from higher ℓ-values is approximated by extrapolation. This might be the reason for the differences of 0.24 eV and 0.17 eV, for the total Coulomb and Breit contributions respectively, compared to the present RMBPT calculation where $\ell_{\max} = 10$ for the Coulomb correlation and $\ell_{\max} = 6$ for the Breit correlation are included.

The difference between the QED calculation of Cheng and Chen [3] and the present work is of the order of 0.7 eV. It is most likely due to two causes. The first one is that Cheng and Chen do a direct calculation of the self-energy with the potential they use to define their wave function, thus obtaining the two-electron radiative corrections directly as a screening effect to the full one-electron radiative corrections. While not a substitute to a full evaluation of second order diagrams pertaining to the two-electron self-energy, it is probably a slightly better method than ours. The second cause is that Cheng and Chen do not include second-order one-electron radiative corrections, which contribute by ≈ 0.1 eV to the difference between the two calculations.

4 Comparison with experiment and discussion

4.1 Comparison with experiment for Th and U

In Table 10 we present a list of the theoretical and experimental energies for both uranium and thorium. This table shows all transitions observed in references [1] and [2], for the $2s_{1/2} - 2p_{3/2}$ electric dipole transitions and charge states from U^{89+} to U^{82+}, and from Th^{87+} to Th^{80+}. The transitions within each charge state were ordered according to the uranium transition energies.

It is very important to compare Th and U to establish the different line identifications. Such an identification should not be based on a single observation. Although our rate calculation shows that the observed lines are indeed the most intense ones, there are certainly many production mechanisms beyond the ones considered here that could result in enhancing other transitions. Also some lines are close enough to each other so that attribution could be problematic. However, if such a misidentification was done, the variation with Z of the theory-experiment difference would change faster than for correctly identified lines.

We performed here the standard line identification procedure, which is to check that the experiment-theory (observed-calculated or o-c) is a slowly varying function of Z. In Figure 1 we plot o-c for Th and U, and a Dirac-Fock calculation which include only one LS configuration. Differences between our best MCDF theoretical and experimental energy in thorium and uranium are plotted in Figure 2. In both cases the o-c differences are identical for Th and U, within the experimental uncertainty, except for the Ne line for which the o-c difference changes by 1.24 ± 0.56 eV.

From both figures we can be very confident that all identifications, except may be for Ne and C (for which changes between U and Th are slightly too large), are correct. However there are no other lines among the 41 which in principle could be possible candidates to replacements in the present identification. One can find better matches, but not with the same candidate for both Th and U. This should be a mandatory criterium, as it would be difficult to accept the possibility of very different population mechanisms for Th and U. In both cases the variation of

Table 10. Comparison between theoretical and experimental energies for uranium and thorium ions. See Table 1 for definitions of Key. In the case of the uranium ions, measured energies $E_{\rm exp}$ and corresponding experimental keys, $\rm Key_{exp}$, are from reference [1]. $\Delta E = E - E_{\rm exp}$ and the values listed under $\Delta E_{\rm A}$, $\Delta E_{\rm B}$, $\Delta E_{\rm C}$, $\Delta E_{\rm D}$ are, respectively, the differences between the following theoretical values and experimental ones: $E_{\rm A}$ are MCDF-Grant calculations from reference [1], $E_{\rm B}$ and $E_{\rm C}$ are the MBPT-A and MBPT-B, respectively, calculations from reference [4] and $\Delta E_{\rm D}$ are CI-DS calculations from reference [3]. In the case of thorium ions, measured energies $E_{\rm exp}$ and corresponding experimental keys, $\rm Key_{exp}$, are from reference [2]. $\Delta E = E - E_{\rm exp}$ and the $\Delta E_{\rm A} = E_{\rm A} - E_{\rm exp}$, where $E_{\rm A}$ are MCDF-Grant calculations from reference [2].

		U						Th			Bi	
Key	$\rm Key_{exp}$	$E_{\rm exp}$ [a]	ΔE	$\Delta E_{\rm A}$	$\Delta E_{\rm B}$	$\Delta E_{\rm C}$	$\Delta E_{\rm D}$	$E_{\rm exp}$ [b]	ΔE	$\Delta E_{\rm A}$	$E_{\rm exp}$ [c]	ΔE
Li	*Li*	4459.37 ± 0.35	0.63	2.3	0.12	−0.24	−0.06	4025.23 ± 0.15	0.62	1.80	2788.139 ± 0.018	0.33
Be	*Be*	4501.72 ± 0.27	−0.18	3.6	1.16	2.56	−0.19	4068.47 ± 0.13	−0.26	3.20		
B1	*B1*	4521.39 ± 0.60	0.70	3.4			−0.09	4089.92 ± 0.50	1.00	3.40		
B2	*B2*	4521.39 ± 0.60	0.98	3.4			0.14	4089.92 ± 0.50	0.84	3.00		
C5	*C*	4548.32 ± 0.20	2.24	4.0	0.07	−0.36	−0.02	4118.43 ± 0.13	1.64	3.70		
N1	*N1*	4440.82 ± 0.20	−0.25	3.1			−0.08	4016.67 ± 0.14	−0.38	2.30		
N9	*N2*	4586.55 ± 0.58	0.39	4.8			0.46	4157.20 ± 0.28	0.57	4.30		
N10	*N3*	4588.73 ± 0.26	0.85	4.5			−0.09	4159.49 ± 0.23	0.85	3.90		
O1	*O1*	4525.26 ± 0.25	0.84	4.0			−0.39	4099.60 ± 0.20	0.08	3.80		
O3	*O2*	4556.42 ± 0.48	2.07	3.8			0.18	4129.94 ± 0.17	−0.20	3.30		
O6	*O3*	4641.76 ± 0.21	1.36	5.5			0.02	4212.80 ± 0.14	0.63	4.60		
F	*F*	4593.83 ± 0.17	1.00	6.0	0.48	0.19	−0.16	4168.06 ± 0.16	0.99	4.60		
Ne3	*Ne*	4630.93 ± 0.33	4.14	8.0	1.92	1.77		4204.92 ± 0.45	2.90	5.50		

[a] Beiersdorfer *et al.* [1].
[b] Beiersdorfer *et al.* [2].
[c] Beiersdorfer *et al.* [61].

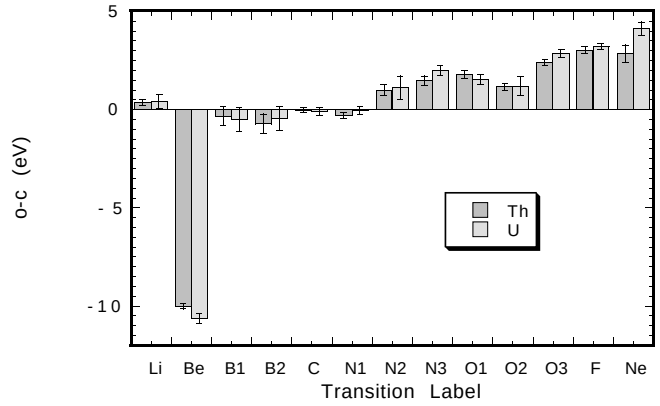

Fig. 1. Observed-Calculated (o-c) plot with Single configuration Dirac-Fock calculation for Th and U ions. The transitions are label with the experimental keys from reference [2].

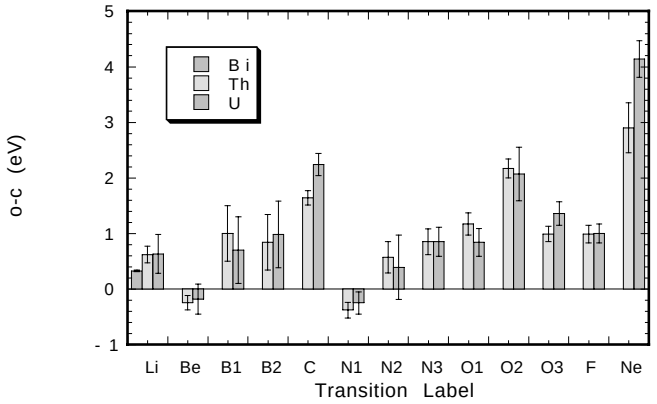

Fig. 2. Observed-Calculated (o-c) plot with Multi Configuration Dirac-Fock calculation for Th and U ions. The transitions are label with the experimental keys from reference [2].

energy differences between Th and U is more than twice the combined experimental error bars.

The calculation for Ne-like ions as presented is much less accurate than the others for a very specific reason. It happens that a very strong contribution to the $1s^22s2p^6$ $3s\ ^1S_0$ level comes from the $1s^22s^22p^53p\ ^3P_0$, which is very close in energy. But because of its symmetry, this configuration prevents convergence even with the most sophisticated methods. In fact it does not converge, even when evaluated as a single configuration. Therefore, we basically did not add any correlation to the Ne transitions, because the imbalance between initial and final state was too large.

4.2 Detailed study of the Oxygen isoelectronic sequence

Because the difference in Z between Th and U is small, we have looked for isoelectronic sequences that could be observed on a wider range. Finally we found experimental data [60] for oxygenlike lines and made an o-c plot in Figure 3 for the oxygen lines with Z ranging from 20 to 92. The calculation in this case has been done with the same set of configuration in the whole range. The o-c energy difference varies relatively smoothly with Z. In Figure 4 we have plotted the correlation energy for initial and final states used in the calculation of the oxygen isoelectronic sequence. One can easily notice the strong variation of the final state correlation with Z. This strong variation is due

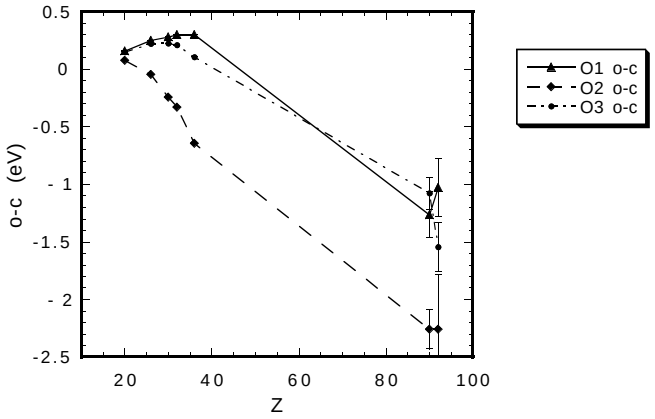

Fig. 3. Observed-Calculated (o-c) plot for $O1$, $O2$, and $O3$ lines for $20 \leq Z \leq 92$. The transitions are labeled with the experimental keys from reference [2].

to the large change of the mixing coefficients between the $1s^2 2s^2 2p^4$ and the $1s^2 2s^2 2p^2 3d^2$ configurations as a function of Z.

We would like to correct a conclusion of references [1,2]. In both papers the authors performed EAL (Extended Average Levels) MCDF calculations with the code of Grant and collaborators. They observed large discrepancies between their calculation and the experimental data (up to 8 eV). This discrepancy is attributed by them to correlation and QED effects. They conclude that the MCDF method is not adequate for these calculations. This conclusion is repeated in the theoretical paper of Cheng and Chen [3]. Here we have proven (see for example Figs. 1 and 2) that the MCDF method in OL (Optimized Levels) mode, with the Welton approximation for self-energy screening reproduces rather well the experimental energies, and is more efficient than RMBPT for ions far from closed shell configurations. The unsatisfactory agreement with the MCDF calculation comes from the EAL approximation and the inadequate self-energy screening (using average orbital radius to define an effective Z to evaluate the self-energy).

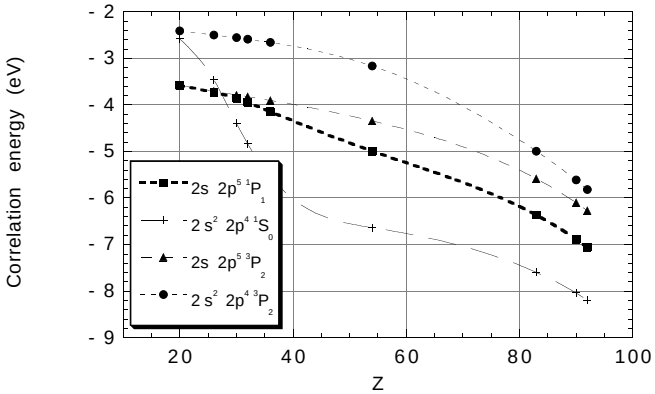

Fig. 4. Correlation contribution to the initial and final states used in the calculation of the oxygen isoelectronic sequence.

Although, there are no experimental (except for lithiumlike ions [61]) or theoretical data on the $2s_{1/2} - 2p_{3/2}$ transitions in bismuth ions, we have extended our calculations to this transitions in order to see if the charge states of this ion have the same structure as the correspondent charge states of the uranium and thorium ions discussed above. A measurement of Bi could help resolve the problem discussed at the beginning of this section.

In Table 7 our theoretical data of the $2s_{1/2} - 2p_{3/2}$ transitions in Bi^{80+} trough neonlike Bi^{73+} (in eV) are presented. We observe that the relative position of the transition energies in boronlike, Bi^{78+}, and carbonlike, Bi^{77+}, charge states are not the same as in uranium and thorium ions, which means that those levels are very sensitive to the charge of the nucleus.

5 Conclusion

We have presented theoretical calculations performed with the MCDF method, including QED effects and contributions from correlation, for $2s_{1/2} - 2p_{3/2}$ transition energies of the charge states lithiumlike Bi^{80+} trough neonlike Bi^{73+}, lithiumlike Th^{87+} trough neonlike Th^{80+} and lithiumlike U^{89+} trough neonlike U^{82+}. The excitation cross sections and transition probabilities were computed for the same cases using MCDF wave functions in monoconfiguration only and the length gauge result was adopted. Forty one allowed electric dipole transitions for the charge states of each ion were calculated. In the studied uranium and thorium ions we confirmed that only the thirteen experimental observed transitions have non-negligible intensities. All forty one transitions for bismuth ions were calculated for the first time. The present bismuth calculations thus serve as reference for future experiments with this ion.

The results were compared with the experimental data available for the uranium and thorium ions. In general, our transition energies agree with the experimental values to a level less than 1 eV, with the exception of the neonlike case. These good results prove that the MCDF method, with small number of configurations, and the Welton approximation for the self-energy screening, is flexible and precise. It can be outperformed by RMPBT for ions close to a closed shell configuration, and by sophisticated RCI methods. The latter however would fail for number of electrons larger than 10, because of the computer resources required to do them. The present MCDF code, because of its flexibility also allowed to predict the existence of several more transitions in the experimental window and to evaluate their intensity, showing that a slightly more sensitive experiment could detect several more lines.

Because of the difficulty inherent to all methods, a scheme combining advance MCDF and RMBPT features is most likely to provide the most general method to solve with high accuracy problems like the one presented here.

The MCDF calculations presented in this work have been done using the computer facilities at the Centro de Física Atómica

da Universidade de Lisboa and at the Laboratoire de Physique Atomique et Nucléaire (LPAN). This research was supported in part by JNICT (Portugal) under project Praxis/2/2.1/FIS/7223/94. One of us, J. P. Santos, acknowledges support from the Embassy of France in Portugal and JNICT for his stay in the LPAN.

References

1. P. Beiersdorfer *et al.*, Phys. Rev. Lett. **71**, 3939 (1993).
2. P. Beiersdorfer *et al.*, Phys. Rev. **A 52**, 2693 (1995).
3. K. Cheng, M. Chen, Phys. Rev. **A 53**, 2206 (1996).
4. W.R. Johnson, J. Sapirstein, K.T. Cheng, Phys. Rev. **A 51**, 297 (1995).
5. I.P. Grant *et al.*, Comput. Phys. Commun. **21**, 207 (1980).
6. B.J. McKenzie, I.P. Grant, P.H. Norrington, Comput. Phys. Commun. **21**, 233 (1980).
7. J.P. Desclaux, Comput. Phys. Commun. **9**, 31 (1975).
8. O. Gorceix, P. Indelicato, J.P. Desclaux, J. Phys. *B*: At. Mol. Phys **20**, 639 (1987).
9. P. Indelicato, O. Gorceix, J.P. Desclaux, J. Phys. **B**: At. Mol. Phys **20**, 651 (1987).
10. P. Indelicato, Nucl. Instrum. Methods Phys. Res. *B* **31**, 14 (1988).
11. P. Indelicato, F. Parente, R. Marrus, Phys. Rev. **A 40**, 3505 (1989).
12. P. Indelicato, Phys. Rev. Lett. **77**, 3323 (1996).
13. J. Olsen *et al.*, Phys. Rev. **E 52**, 4499 (1995).
14. F.A. Parpia, M. Tong, C. Froese Fischer, Phys. Rev. **A 46**, 3117 (1992).
15. A. Ynnerman, C. Froese Fischer, Phys. Rev. **A 51**, 2020 (1995).
16. J. Bieron, P. Jönsson, C. Froese Fisher, Phys. Rev. **A 53**, 1 (1996).
17. T. Mooney *etal.*, Phys. Rev. **A 45**, 1531 (1992).
18. P. Indelicato, E. Lindroth, Phys. Rev. **A 46**, 2426 (1992).
19. G.E. Brown, D.E. Ravenhall, Proc. R. Soc. London, Ser **A 208**, 552 (1951).
20. J. Sucher, Phys. Rev. **A 22**, 348 (1980).
21. P. Indelicato, Phys. Rev. **A 51**, 1132 (1995).
22. I.P. Grant, H.M. Quiney, Adv. At. Mol. Phys. **23**, 37 (1988).
23. J.P. Desclaux, in *Methods and Techniques in Computational Chemistry* (STEF, Cagliary, 1993), Vol.A.
24. I.P. Grant, B.J. McKenzie, J. Phys. **B**: At. Mol. Phys **13**, 2671 (1980).
25. I.P. Grant, J. Phys. **B**: At. Mol. Phys **20**, L735 (1987).
26. J.L. Heully *et al.*, J. Phys. **B**: At. Mol. Phys **19**, 2799 (1986).
27. J.L. Heully, I. Lindgren, E. Lindroth, A.M. Mårtensson-Pendrill, Phys. Rev. **A 33**, 4426 (1986).
28. C. Froese Fisher, *The Hartree-Fock Method for Atoms* (Wiley, New York, 1977).
29. J.P. Desclaux, P. Indelicato, Y.-K. Kim, F. Parente (unpublished).
30. P.J. Mohr, Ann. Phys. (N. Y.) **88**, 26 (1974).
31. P.J. Mohr, Ann. Phys. (N. Y.) **88**, 52 (1974).
32. P.J. Mohr, Phys. Rev. **A 26**, 2338 (1982).
33. P.J. Mohr, Y.-K. Kim, Phys. Rev. **A 45**, 2727 (1992).
34. P.J. Mohr, G. Soff, Phys. Rev. Lett. **70**, 158 (1993).
35. E.A. Uehling, Phys. Rev. **48**, 55 (1935).
36. G. Soff, P.J. Mohr, Phys. Rev. **A 40**, 2174 (1989).
37. G. Soff, P.J. Mohr, Phys. Rev. **A 38**, 5066 (1988).
38. H. Persson, I. Lindgren, S. Salomonson, P. Sunnergren, Phys. Rev. **A 48**, 2772 (1993).
39. I. Lindgren *et al.*, J. Phys. **B**: At. Mol Phys. **26**, L503 (1993).
40. K. Pachucki, Phys. Rev. Lett. **72**, 3154 (1994).
41. H. Person, *et al.*, Phys. Rev. **A 54**, 2805 (1996).
42. G. Källén, A. Sabry, Mat. Fys. Medd. Dan. Vid. Selsk. **29**, 17 (1955).
43. P. Indelicato, P.J. Mohr, Theor. Chim. Acta **80**, 207 (1991).
44. H. Persson, S. Salomonson, P. Sunnergren, I. Lindgren, Phys. Rev. Lett. **76**, 204 (1996).
45. K.T. Cheng, W.R. Johnson, J. Sapirstein, Phys. Rev. Lett. **66**, 2960 (1991).
46. S.A. Blundell, Phys. Rev. **A 46**, 3762 (1992).
47. S.A. Blundell, Phys. Rev. **A 47**, 1790 (1993).
48. P. Indelicato, J.P. Desclaux, Phys. Rev. **A 42**, 5139 (1990).
49. S.A. Blundell, Phys. Scr. **T46**, 144 (1993).
50. G. Plunien, B. Müller, W. Greiner, G. Soff, Phys. Rev. **A 39**, 5428 (1989).
51. G. Plunien, G. Soff, Phys. Rev. **A 51**, 1119 (1995).
52. G. Plunien, G. Soff, Phys. Rev. **A 53**, 4614 (1996).
53. D.H. Baik *et al.*, At. Data Nucl. Data Tables **47**, 177 (1991).
54. Y.-K. Kim, M. Inokuti, Phys. Rev. **A 3**, 665 (1971).
55. Y.-K. Kim, K.-T. Cheng, Phys. Rev. **A 18**, 36 (1978).
56. Y.-K. Kim, M.E. Rudd, Phys. Rev. **A 50**, 3954 (1994).
57. P. Indelicato, E. Lindroth, Phys. Rev. **A 46**, 2426 (1992).
58. S. Salomonson, P. Öster, Phys. Rev. **A 40**, 5548 (1989).
59. S. Salomonson, P. Öster, Phys. Rev. **A 41**, 4670 (1990).
60. *National Institute of Standards and Technology Atomic Spectroscopic Database*, available on the URL http://aeldata.phy.nist.gov/nist_atomic_spectra.html.
61. P. Beiersdorfer *et al.*, preprint UCRL-JC-127437 (unpublished).